# Modeling and Simulation of Line Edge Roughness for EUV Resists

**Sang-Kon Kim**

*Abstract*—**With the extreme ultraviolet (EUV) lithography, the performance limit of chemically amplified resists has recently been extended to 16- and 11-nm nodes. However, the line edge roughness (LER) and the line width roughness (LWR) are not reduced automatically with this performance extension. In this paper, to investigate the impacts of the EUVL mask and the EUVL exposure process on LER, EUVL is modeled using multilayer-thin-film theory for the mask structure and the Monte Carlo (MC) method for the exposure process. Simulation results demonstrate how LERs of the mask transfer to the resist and the exposure process develops the resist LERs.**

*Index Terms*—**Lithography, lithography simulation, LER, EUVL, EUV mask, Monte Carlo**

## I. INTRODUCTION

The extreme ultraviolet lithography (EUVL) with the 13.5-nm wavelength is expected to become mainstream for the semiconductor device production process for 16-nm half pitch and below. The international technology roadmap for semiconductors (ITRS) requires less than 3-nm line edge roughness (LER) for the 30-nm pattern size. However, the surface roughness of sidewalls and sizes of patterned resists, called LER, do not reduce automatically with respect to the resolution, so LER can become the most important issue [1]. EUVL has many characteristics in common with conventional optical lithography, but a multilayer reflective mirror has to be used in EUVL, instead of a refractive lens, due to the high absorption in the material. EUVL masks require high reflectivity from the mask and are fabricated by depositing reflective Mo/Si multilayer films onto super-polished substrates. Mask LER, which can easily be produced on the multilayer EUVL mask, can alter the reflected near-field image and the aerial image on the resist [2, 3]. During the resist process, many materials of resists and process factors affect LER because LER is formed from a chemical inhomogeneity at the boundary between the soluble and insoluble regions [4, 5]. Modeling of the EUVL can help us to understand the phenomena of EUVL, to overcome the drawbacks such as buried defects in EUV masks and shadowing effects due to reflectivity of the mask and oblique illumination, and to optimize mask structure and process parameters. Ultimately, the simulator tool can help to develop new mask materials and new resists. For these purposes, the LER modeling of EUVL has been actively researched for half a decade. However, this research has been developed with unclear and restricted modeling results.

In this paper, a new attempt to simulate EUVL mask is introduced to describe the transfer of mask LER onto a wafer, using multilayer-thin-film theory. To reduce LER, the near-field image of EUVL mask and the internal concentrations of resist processes are analyzed. The LER formations of the Monte Carlo (MC) simulation in a 193-nm resist are compared with those of an EUV. The limit of LER at high exposure dose was theoretically investigated on the basis of EUV sensitization mechanisms.

Manuscript received Apr. 26, 2012; accepted Dec. 11, 2013
Department of Applied Physics, Hanyang University, Ansan 426-791, Korea
E-mail: sangkona@hotmail.com, sangkon@hanyang.ac.kr, www.sangkon.info

## II. Line Edge Roughness of Mask

For the modeling of EUV processes, as shown in Fig. 1, the schematic representation of EUV light source, reflective mask, condenser optics, and reflective projection optics can be modeled into the structures of the mask simulation (angle of incidence, electric field calculation, absorber shape, and multilayer) and projection illumination (numerical aperture (NA), σ, dose, defocus, and aberrations) [6, 7]. Resist processes are modeled in stages of prebake (Dill parameters (A and B), time, and temperature), exposure (Dill parameters (A, B, and C) and dose), post-exposure bake (diffusion coefficient, time, and temperature), and development (rate function time and surface inhibitor) [8, 9].

For the mask simulation, mask materials are composed with a complex index of refraction $N_j$ (= $n - ik$, where $n$ is the real refractive index and $k$ is the imaginary refractive index), which depends on the mask properties and the relative inhibitor concentration ($M$) of the layer.

The intensity of layer $j$ at $t = 0$ using Dill's model is

$$\frac{\partial I(x,z,t)}{\partial z} = -\alpha I(x,z,t) \rightarrow$$
$$I_j = I_{j-1}\exp\left[-(AM+B)\delta z\right], \quad (1)$$

$$\frac{\partial M(x,z,t)}{\partial t} = -CI(x,z,t)M(x,z,t) \rightarrow$$
$$M_j = M_{j-1}\exp\left[-I_j Ct\right], \quad (2)$$

where $I$ is the intensity, the optical absorption coefficient α is $AM(x,z,t) + B$, $A$ , $B$, and $C$ are Dill's parameters, and δz is the thickness of the mask. When $M$ changes roughly the same with each energy increment, the relation between the energy absorbed in the layer ($E$) and the relative inhibitor concentration ($M$) using Eqs. (1) and (2) can be

$$M_{k-1} - \delta M_k = \exp\left[\left(E_{k-1} - \delta E_k\right)K_d\right], \quad (3)$$
$$K_d = -I_{rel} \bullet C\exp\left[(A+B)d\right], \quad (4)$$

where $d$ is the thickness of the resist, $M_{k-1}$ is the value of $M$ at the end of the $k$-$1$-th energy exposure increment, $\delta M$ is the change in $M$ that the $k$-th energy increment $\delta E_k$ produces, and $I_{rel}$ refers to the relative intensity. The absorption energy for each layer using Eq. (2) is

$$\delta E_k = \frac{\ln\left(M_{k-1} - \delta M_k\right)}{-I_{rel} \bullet C\exp\left[-(A+B)d\right]} - E_{k-1}. \quad (5)$$

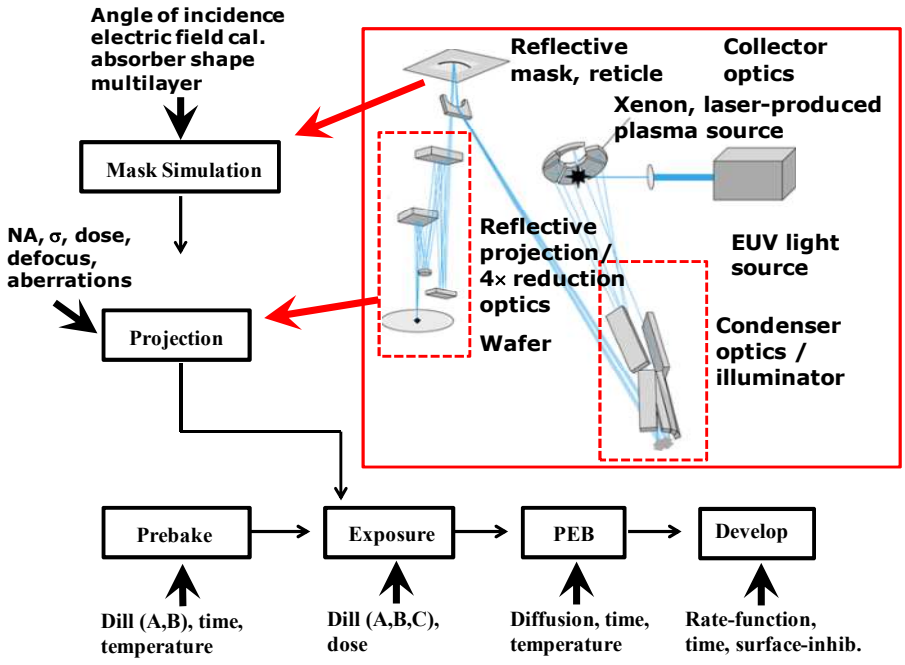


**Fig. 1.** Schematic structure flow of EUV processes: schematic representation of EUV light source, reflective mask, condenser optics, and reflective projection optics in a rectangle box and the modeled structures of mask simulation, projection illumination, prebake, exposure, post exposure bake (PEB), and development.

From Berning's theory for thin film optics, the reflectance and the transmittance are

$$r_{j-1}=\frac{e^{-i2\varphi_j}\left(F_j-r_j\right)-F_j\left(1-F_jr_j\right)}{F_je^{-i2\varphi_j}\left(F_j-r_j\right)-\left(1-F_jr_j\right)},$$
$$t_{j-1}=\frac{\left(F_j^2-1\right)t_je^{-i\varphi_j}}{F_je^{-i2\varphi_j}\left(F_j-r_j\right)-\left(1-F_jr_j\right)} \quad (6)$$

where $t_m=2\sqrt{n_0 real\left(N_{m=1}\right)}\Big/\left(n_0-N_{m+1}\right)$ for the last layer $m$ in the resist, $r_m=F_{m+1}$, $\varphi_j=i\left[2\pi/\lambda_0\, N_jd_j\right]$, $F_j=n_0-N_j\Big/\left(n_0+N_j\right)$, and $n_0$ is the real refractive index in the medium above the resist. The ratio of the power absorbed in the *j*-th layer to the power absorbed in the *j-1*-th layer is given using

$$\frac{P_j}{P_{j-1}}=\frac{\left|t_{j-1}\right|^2\left(1-\left|r_j\right|^2\right)}{\left|t_j\right|^2\left(1-\left|r_{j-1}\right|^2\right)}. \quad (7)$$

The power absorbed in the *j*-th layer, by Eq. (1), is

$$A_j=\frac{I_{j-1}-I_j}{I_0}=\frac{I_{j-1}}{I_0}\left(AM+B\right)\delta z. \quad (8)$$

The relative inhibitor concentration *M* of Eq. (2) by Eq. (6) can be rewritten as

$$M=M_0\exp\left[-\frac{A_jC\delta E}{\left(AM+B\right)\delta z}\right], \quad (9)$$

where the intensity *I* is $I_{j-1}/I_0$ [10, 11].

For the optical projection system, the Kohler's method is implemented to forms an image of mask reflectance onto the projection lens. The intensity on wafer can be

$$I(\vec{r}_i)=\left[\iint TCC(\vec{\rho}_P;\vec{\rho}'_P)\tilde{M}(\vec{\rho}_P)\tilde{M}^*(\vec{\rho}'_P)e^{-2\pi i(\vec{\rho}_P-\vec{\rho}'_P)\cdot\vec{r}_i}d^2\vec{\rho}_Pd^2\vec{\rho}'_P\right], \quad (10)$$

$$TCC=\int\tilde{J}_0\left(\vec{\rho}_C\right)\cdot\tilde{K}\left(\vec{\rho}_C+\vec{\rho}_P\right)\cdot\tilde{K}^*\left(\vec{\rho}_C+\vec{\rho}'_P\right)d^2\vec{\rho}_C, \quad (11)$$

where $\rho_P$ (= (f, g)) is a normalized spatial frequency divided by NA/λ, NA is numerical aperture, *TCC* is the transmission cross coefficients, $J\left(\vec{r}_i\right)$ is mutual intensity, $M\left(\vec{r}_0\right)$ is mask reflection function, and $K\left(\vec{r}_i\right)$ is transfer function of projection lens. In the diffraction of circular aperture, the Fourier transfer function of the mutual intensity is

$$J_0\left(\vec{r}_0-\vec{r}'_0\right)=\int\tilde{J}_0\left(\vec{\rho}_C\right)e^{i2\pi(\vec{r}_0-\vec{r}'_0)\cdot\vec{\rho}_C}d^2\vec{\rho}_C,$$
$$\tilde{J}_0\left(\vec{\rho}_C\right)=\begin{cases}\dfrac{\lambda^2}{\pi NA_C^2}\Gamma_0=\dfrac{\lambda^2}{\pi\sigma^2NA_P^2}, & \left|\vec{\rho}_C\right|\langle\dfrac{NA_C}{\lambda}=\dfrac{\sigma NA_P}{\lambda}\\ 0, & otherwise\end{cases}. \quad (12)$$

The Fourier transfer function of the mask reflection function with reflectance at each of mask points is

$$M\left(\vec{r}_0\right)=R\left(\vec{r}_0\right)e^{i\Phi(\vec{r}_0)}=\int_\Omega\tilde{M}\left(\vec{\rho}_P\right)e^{2\pi i\vec{\rho}_P\cdot\vec{r}_0}d\vec{\rho}_P, \quad (13)$$

where *R* is reflectance function. The Fourier transfer function of the transfer function of projection lens is

$$K\left(\vec{r}_i-\vec{r}'_0\right)=\int\tilde{K}\left(\vec{\rho}_P\right)e^{i2\pi(\vec{r}_i-\vec{r}'_0)}d^2\vec{\rho}_P,$$
$$\tilde{K}\left(\vec{\rho}_P\right)=\begin{cases}e^{-i\frac{2\pi}{\lambda}W(\vec{\rho}_P)}, & \left|\vec{\rho}_P\right|\langle\dfrac{NA_P}{\lambda},\\ 0, & otherwise\end{cases} \quad (14)$$

where the wavefront aberration of imaging illumination is $W\left(\vec{\rho}\right)=\sum_{l,m,n}C_{lmn}\left(\left|\vec{r}\right|^2\right)^l\left(\vec{r}\cdot\vec{\rho}\right)^m\left(\left|\vec{\rho}\right|^2\right)^n$ [12].

The basic structure of a EUVL mask is shown in Fig. 2(a). The mask consists of Cr absorber and Mo/Si multi-layers on a base substrate. The simulation range is 100-nm (x-axis) × 100-nm (z-axis). Table 1 summarizes the properties of the mask stacks and illumination conditions. The angle incidence of illumination is 0° in order to ignore the shadow effect of the illumination angle. The near-fields reflected from the mask and the aerial images are calculated based on the changing of the mask edge slope. For the mask shown in Fig. 2(a), the mask edge slope is the low frequency pattern and the saw-like shape of the mask edge slope is the high frequency pattern. In

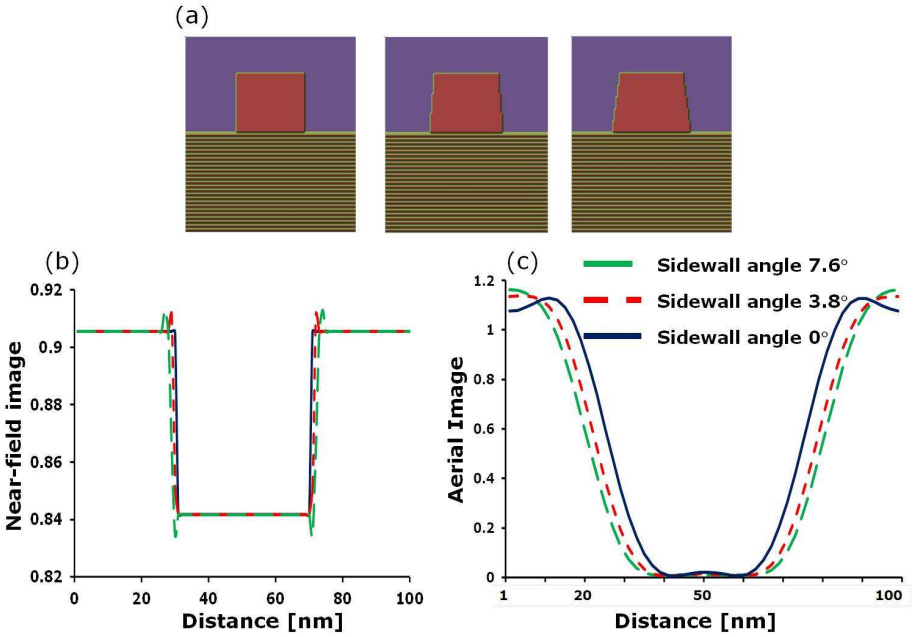


**Fig. 2.** Modeling and simulation results of a EUVL mask (a) a basic structure of a EUVL mask, (b) reflectance, (c) aerial images of a 40-nm absorber pattern.

**Table 1.** Simulation condition of EUVL mask

| Parameter | Value |
|---|---|
| Radiation wavelength (l) | 13.5-nm |
| Angle incidence (q) | 0 deg |
| Absorber index of refraction ($n_{Cr}$) | 0.932763+i 0.038639 |
| Absorber thickness ($h_{Cr}$) | 70-nm |
| Absorber width (w) | 25-nm |
| Mo index of refraction ($n_{Mo}$) | 0.921838 + i 0.006334 |
| Mo thickness ($h_{Mo}$) | 2.8-nm |
| Si index of refraction ($n_{Si}$) | 0.9995537 + i 0.001824 |
| Si thickness ($h_{Si}$) | 4.1-nm |
| Background index of refraction ($n_{Inc}$) | 1.00 |
| Substrate index of refraction ($n_{Sub}$) | 0.9995537 + i 0.001824 |
| Number of layers (N) | 40 |
| Numerical Aperture (NA) | 0.25 |
| Reduction | 0.25 |
| Coherence (s) | 0.5 |

the near-field image of the EUVL mask shown in Fig. 2(b), although the saw-like shape has disappeared, the mask edge slope and its saw-like shape are changed into the slope of the near-field image and the peaked field image, respectively. In the aerial image of the EUVL mask shown in Fig. 2(c), the slope of the near-field image and its peaked field image are transferred into the slope of the aerial image. For the mask LER, the low frequency mask roughness is expected to be fully transmitted onto the wafer, but the high frequency mask roughness is not transmitted onto the wafer.

## III. Line Edge Roughness of Resist Process

Fig. 3 shows simulation flow of EUV resist processes, which include spin-coating, prebake, projection, exposure, and development.

Fig. 4 shows the simulation results of spin-coating, projection, exposure, PEB, and development for a 31-nm isolated line pattern with 85.52° sidewall angle in a 193-nm resist. Simulation parameters are described in Table 2. LER is inversely proportional to the concentration gradient of the molecules that determine the solubility of the resist (chemical gradient) [13, 14]. Since the LER of resist processes is determined by various chemical components during resist processes, LER equations can be assumed that

$$\sigma_{LER} = \frac{\sigma_I}{dI/dx} + \sigma_0 \quad \text{for intensity,} \tag{15}$$

$$\sigma_{LER} = \frac{\sigma_{[PAG]}}{d[PAG]/dx} + \sigma_0 \quad \text{for PAG,} \tag{16}$$

$$\sigma_{LER} = \frac{\sigma_{[Acid]}}{d[Acid]/dx} + \sigma_0 \quad \text{for acid,} \tag{17}$$

$$\sigma_{LER} = \frac{\sigma_{[M]}}{d[M]/dx} + \sigma_0 \quad \text{for M,} \tag{18}$$

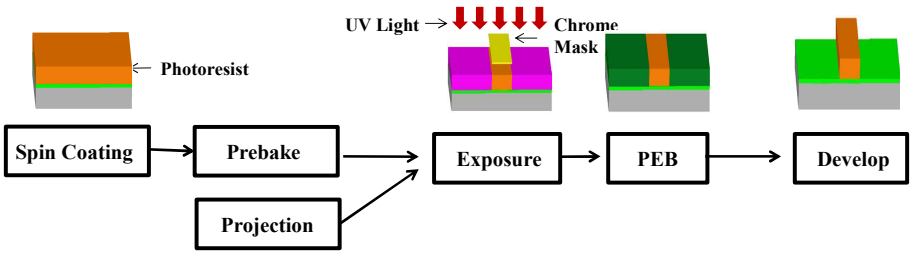


**Fig. 3.** Simulation structure flow of EUV resist processes, which are spin-coating, prebake, projection, exposure, and development.

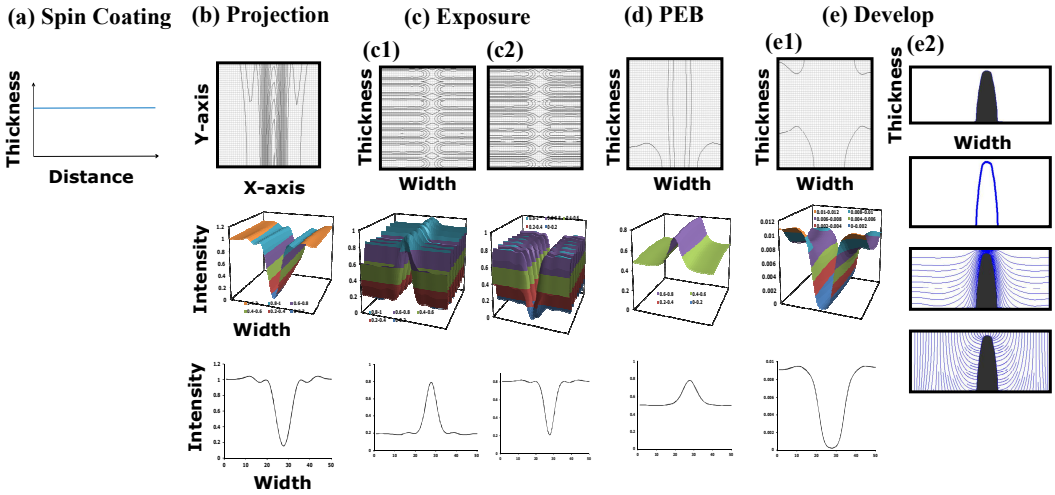


**Fig. 4.** Simulation results for a 31-nm isolated line (a) resist thicknesses after spin-coating, (b) intensity distributions on wafer after projection, (c1) photo acid generator (PAG) concentrations, (c2) photo acid concentrations after exposure, (d) cross-linked polymer concentrations after post exposure bake (PEB), (e1) develop rate concentrations, (e2) pattern profiles after development.

$$\sigma_{LER} = \frac{\sigma_{[R]}}{d[R]/dx} + \sigma_0 \quad \text{for R,} \tag{19}$$

$$\sigma_{LER} = \frac{\sigma_{[Side\ Angle]}}{[Side\ Angle]} + \sigma_0 \quad \text{for sidewall angle.} \tag{20}$$

where $I$ is intensity, $x$ is distance, $\sigma_0$ is constant, $\sigma_{[PAG]}$, $\sigma_{[Acid]}$, $\sigma_{[M]}$, $\sigma_{[R]}$, and $\sigma_{[Side\ Angle]}$ are LERs of the photoacid generator (PAG), acid, the cross-linked polymer concentration (M), the develop rate concentration (R), and the side angle of the development profile, respectively.

Fig. 5 shows the resist LERs of PAG in Fig. 4(c1), $M$ in Fig. 4(d), $R$ in Fig. 4(e1), and sidewall angle in Fig. 4(e2) due to exposure doses. Since the chemical gradient increases with the increase of exposure dose, as shown in Fig. 5, LER is inversely decreased. Although comparison of the experimental results with the simulation results is required, the LER slopes of $R$ and the side angle are more sensitive to exposure than are the slopes of PAG and $M$. With the trade-off relationship between LER and sensitivity, LER decreases when sensitivity decreases. However, the decrease of LER is saturated at high exposure dose, and so LER does not converge of 0, shown in Fig. 5. During pattern generation, stochastic effects play a non-negligible role in resist edge placement randomness. One of the stochastic methods is the MC method.

For the confidence of the MC simulation about LER, Fig. 6 shows application of the MC method. The MC method can be successfully used for the deposition of materials from an electrolytic solution at very low voltage, as shown in Fig. 6(a). An illustration of a porous material through which certain particles can diffuse (or percolate) if there are continuous paths through the pores is shown in Fig. 6(b), and a random walk with continuous step sizes and directions, or one on a lattice, is shown in Fig. 6(c) [15, 16].

Fig. 7 shows the schematic comparison of UV-resist interaction and EUV-resist interaction. For the expose

**Table 2.** Parameters of 31-nm isolated line at 193-nm resist

- **Mask pattern**
  35-nm isolated line pattern
- **Modeling options**
  Image Calculation Model: Vector
- **Stepper parameters**
  Illumination: polarized dipole illumination (σ=0.45/0.65, opening angle 35°),
  Defocus: 0.0 mm, Wavelength: 193-nm,
  Numerical Aperture (NA): 1.35, Aberrations: none,
  Flare [%]: 0
- **Film stack**
  Layer 1: 100-nm resist, refraction: 1.72 - j0.02,
  30-nm BARC
  Layer 2: Silicon, refraction: 6.522 - j2.705
  30 nm hard mask 1,
  Resist thickness: 0.39 mm
- **Soft baking parameters**
  Temperature: 120 °C, Time: 60 s
- **Spin-coating parameters**
  Density of the fluid: 1 g/cm$^3$,
  Surface tension of the fluid: 18.59 dyn/cm,
  Radius at the center of the wafer: 2 cm
- **Exposure parameters**
  Litho 1 Dose: 22 mJ/cm$^2$,
  A: 0.01 (1/mm), B: 0.5 (1/mm), C: 0.03 (cm$^2$/mJ),
- **Post exposure baking parameters**
  Diffusion Length: 0.045 mm, Temperature: 100 °C,
  Time: 60 s, Q: 0.05,
  $k_{amp}$(1/s):1.5,$k_{loss}$(1/s):2.3x10$^{-5}$,$k_{quench}$=0.067,
  Resist type: Positive, Exponent n: 2,
- **Development parameters**
  Development Model : enhanced Mack model
  $R_{min}$:2x10$^{-5}$nm/s,$R_{max}$: 0.045 mm/s, n: 1.61
  $R_{res}$:0.0187mm/s, : 9.84, Time: 45 s
- **2D resist profile**
  CD: 31 nm, Average sidewall angle: 85.52°

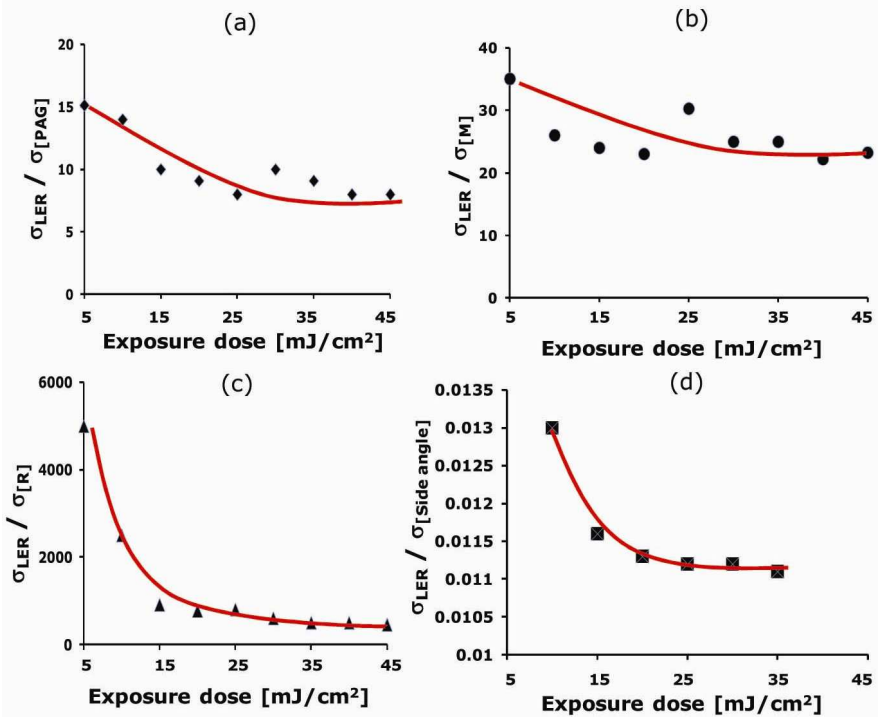


**Fig. 5.** Simulation results of the ratio of Resist LER (a) PAG LER in Fig. 4(c1), (b) M (the cross-linked polymer concentration) LER in Fig. 4(d), (c) R (the develop rate concentration) LER in Fig. 4(e1), (e) LER of sidewall angle in Fig. 4(e2) for exposure doses.

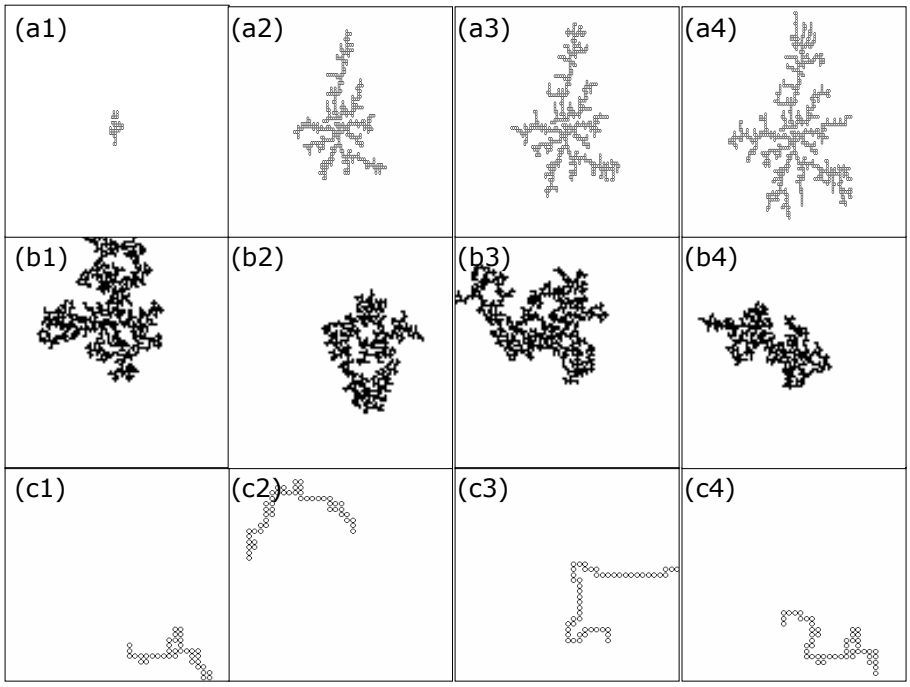


**Fig. 6.** Simulation results of the Monte Carlo method: the diffusion limited aggregation (DLA) clusters on a square lattice with (a1)-(a4) different fractional dimensions and the maximum radial size of the cluster, the percolating clusters at the percolation threshold $p$ = 0.592750, (b1) 579, (b2) 653, (b3) 950, (b4) 1023 cluster sizes, and polymer chains of length $N$ = 50 with (c1)-(c4) different times.

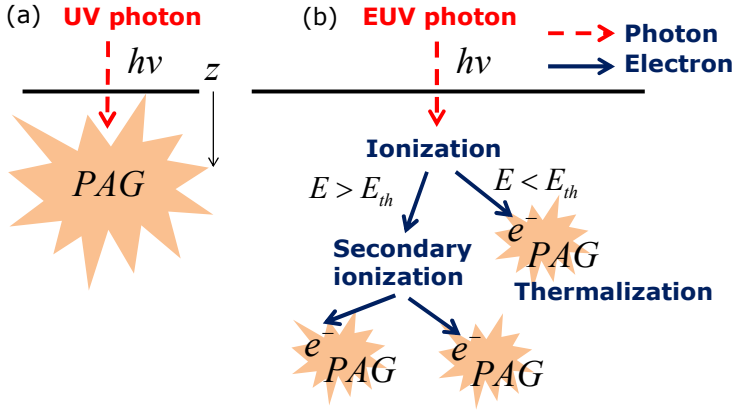


**Fig. 7.** Schematic drawing of (a) UV-resist interaction, (b) EUV-resist interaction.

mechanism of 193-nm photoresists in Fig. 7(a), PAG interacted with a photon generates an acid. For spin-coating process, PAGs are populated in the simulation domain according to the random Poisson statistics. For exposure process, PAG is exposed according to random Poisson statistics and Dill's first-order exposure rate Eq. [16]. Unlike the direct photon absorption mechanism of 193-nm photoresists, the absorption of a photon in an EUV resist leads to ionization, generating an electron (called a photoelectron), which in turn can generate several secondary electrons in terms of excess energy. The mean free path of photoelectrons is less than the diffusion length of acid in 193-nm resists. These electrons then scatter through the resist and, occasionally, interact with a PAG to generate an acid [17-19].

Fig. 8 shows the simulation results for the LER effect of PAG loading and the exposure dose in a 45-nm isolated pattern of a 193-nm resist and in 16-nm and 22-nm isolated patterns of an EUV resist. Simulation parameters are described in Table 3. For the EUV simulation, as shown in Fig. 8(b), the first step is that a light changes into a number of photons in the resist. The

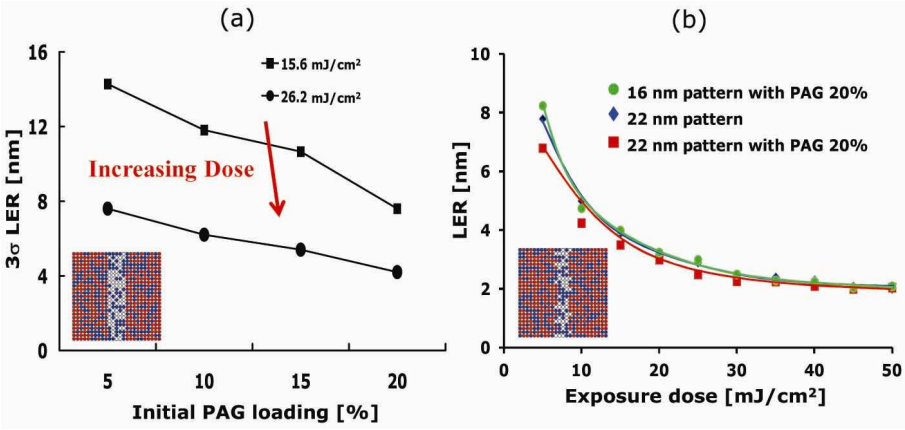


**Fig. 8.** Simulation results of the Monte Carlo method for the LER effect of PAG loading and the exposure dose (a) in a 45-nm isolated pattern of a 193-nm resist, (b) in 16-nm and 22-nm isolated patterns of an EUV resist. Inserted figures are simulation results of a 100-nm × 100-nm domain in Fig. 6(a) and a 50-nm × 50-nm domain in Fig. 6(b) where blue dot is PAG and white dot is acid.

**Table 3.** Resist parameters for 193-nm and EUV simulations

| Parameter | 193-nm | EUV |
|---|---|---|
| Photon energy* | 6.4 eV | 91.8 eV |
| Number of photon/nm$^2$ | 97 | 3 or 4 |
| Exposure rate constant | 0.024741 cm$^2$/mJ | - |
| PAG molar absorptivity | 0 | 0 |
| Initial PAG density | 0.05 nm$^3$ | 0.05 nm$^3$ |
| Ionization potential (IP) | - | 10 eV |
| PAG excitation radius | - | 2.0-nm |
| PAG excitation efficiency | - | 0.5 |
| Electron generation efficiency | - | 0.9 |
| Absorption coefficient a | 0.0015 nm$^{-1}$ | 0.006516 nm$^{-1}$ |
| Open frame area | 100-nm × 100-nm | 50-nm × 50-nm |
| Resist thickness | 50-nm | 10-nm |

* $E = h\nu = \frac{hc}{\lambda} \rightarrow Dose = N_{photon} E = N_{photon} \frac{hc}{\lambda}$

second step is that the photons are converted to electrons with the electron generation efficiency, and the kinetic energy of each electron is the reduction of ionization potential with the photon energy. The third step is that electrons move and interact with components of the resist until they lose energy. In an inelastic collision, the resist is ionized and a secondary electron is ejected. The fourth step is that when electron is within the reaction radius of PAG and the electron energy is greater than the PAG excitation energy, an acid is generated. When the PAG loading and the exposure dose increase, LER is reduced and saturated in Figs. 8(a) and (b).

## IV. Conclusions

For the transfer of the line-edge-roughness (LER) of the extreme ultraviolet lithography (EUVL) mask, the near-field image on the EUVL mask and the aerial image on the wafer are calculated by using multilayer-thin-film theory. Simulation results show that the low frequency mask roughness is fully transmitted onto the wafer, but high frequency mask roughness is not present on the wafer. For the chemical gradient method of a chemically amplified 193-nm resist, the LER slopes of the development rate concentration and side angle are more sensitive to the exposure dose than are those of a photoacid generator and the cross-linked polymer concentration. The LER decrease is saturated at high exposure dose, and LER does not converge of 0. For the Monte Carlo method of 193-nm and EUV resists, according to the increase of the PAG loading and exposure dose, LER is reduced and saturated. For reduction of resist LER, the resist absorption of EUV light should be increased, but the spatial distribution fluctuations of PAG should be reduced.

## REFERENCES


[1] G. M. Gallatin, P. Naulleau, D. Niakoula, R. Brainard, E. Hassanein, R. Matyi, J. Thackeray, K. Spear, and Kim Dean, "Resolution, LER and sensitivity limitations of photoresist," *Proc. of SPIE* Vol.6921, Feb., 2008, pp.69211E.

[2] P. P. Naulleau, "Correlation method for the measure of mask-induced line-edge roughness in extreme ultraviolet lithography," *Appl. Opt.* Vol.48, June, 2009, pp.3302-3307.

[3] P. P. Naulleau and G. M. Gallatin, "Line-edge roughness transfer function and its application to determining mask effects in EUV resist characterization," *Appl. Opt.* Vol.42, June, 2003, pp.3390-3397.

[4] T. Schnattinger and A. Erdmann, "A comprehensive resist model for the prediction of line-edge roughness material and process dependencies in optical lithography," *Proc. of SPIE* Vol.6923, Feb., 2008, pp.69230R.

[5] J. J. Biafore, M. D. Smith, S. A. Robertson, and T. Graves, "Mechanistic simulation of line-edge roughness," *Proc. of SPIE* Vol.6519, Feb., 2007, pp.65190Y.

[6] A. V. Pret and R. Gronheid, "Mask line roughness contribution in EUV lithography," *Microelectron. Eng.* Vol.88, Feb., 2011, pp.2167-2170.

[7] A. R. Pawloski, A. Acheta, I. Lalovic, B. L. Fontaine, and H. J. Levinson, "Characterization of line edge roughness in photoresist using an image fading technique," *Proc. SPIE* Vol.5376, Feb., 2004, pp.414-425.

[8] Y. Kikuchi, Y. Tanaka, H. Oizumi, F. Kumasaka, D. Goo, and I. Nishiyama, "Evluation of resolution and LER in the resist patterns replicated by EUV micro-exposure tools," *Proc. SPIE* Vol.6151, Feb., 2006, pp.615107.

[9] C. A. Fonseca, R. Gronheid, and S. A. Scheer, "Extraction and identification of resist modeling parameters for EUV lithography," *Proc. SPIE* Vol.6923, Feb., 2008, pp.69230T.

[10] S.-K. Kim, "Exposed pattern interaction of litho-cure-litho-etch process in computational lithography," *J. Korean Phys. Soc.* Vol.59, Aug., 2011, pp.425-430.

[11] S.-K. Kim and H.-K. Oh, "Bulk Image Formation of Scalar Modeling in Photoresist," *J. Korean Phys. Soc.* Vol.41, Oct., 2002, pp.456-460.

[12] S.-K. Kim, "Polarized effects in optical lithography with high NA technology," *J. Korean Phys. Soc.* Vol.50, Jun., 2007, pp.1952-1958.

[13] T. Kozawa and S. Tagawa, "Radiation chemistry in chemically amplified resists," Jpn. J. Appl. Phys. Vol.49, Mar., 2010, pp.030001.

[14] B. Wu and A. Kumar, *Extreme Ultraviolet Lithography*, McGraw-Hill Co. Inc., 2009, chapter 7.

[15] W. Kinzel and G. Reents, *Physics by computer*, Springer Press, 1996.

[16] S.-K. Kim, H-K. Oh, Y-D. Jung, and Ilsin An, "Impact of the parameters for a chemically-amplified resist on the line-edge-roughness by using a molecular-scale lithography simulation," *J. Korean Phys. Soc.* Vol.55, Aug., 2009, pp.675-680.

[17] A. Saeki, T. Kozawa, and S. Tagawa, "Relationship between resolution, line edge roughness, and sensitivity in chemically amplified resist of post-optical lithography revealed by Monte Carlo and dissolution Simulations," *Appl. Phys. Express* Vol.2, June, 2009, pp.075006.

[18] C. A. Mack, J. W. Thackeray, J. J. Biafore, and M. D. Smith, "Stochastic exposure kinetics of extreme ultraviolet photoresists: simulation study," *J. Micro/Nanolith. MEMS MOEMS* Vol.10, No.3, July, 2011, pp.033019.

[19] R. A. Lawson, C-T. Lee, W. Yueb, L. Tolbert, and C. L. Henderson, "Mesoscale simulation of molecular glass photoresists: effect of PAG Loading and acid diffusion coefficient," *Proc. SPIE* Vol.6923, Feb., 2008, pp.69230Q.


**Sang-Kon Kim** received B.S. in Physics from Hanyang University in 1985, M.S. in Physics from Northeastern University in 1988, and Ph.D. in Physics from Hanyang University in 2002. He is currently a visiting professor in Applied Physics at Hanyang University. From 1990 to 1993, he was researcher at Samsung Electronics. From 2005 to 2006, he was a visiting professor at Information, Communi- cations and Electronics Engineering in Catholic University. From 2007 to 2011, he was a researcher professor at Hanyang University. His interesting area is lithography process, simulation, lithography CAD, MEMS, and bioMEMS.